

# Confirming the intrinsic abundance spread in the globular cluster NGC 6273 (M 19) with calcium triplet spectroscopy<sup>\*</sup>

David Yong,<sup>1</sup>† Gary S. Da Costa<sup>1</sup> and John E. Norris<sup>1</sup>.

<sup>1</sup>*Research School of Astronomy and Astrophysics, Australian National University, Canberra, ACT 2611, Australia*

2 April 2021

## ABSTRACT

We present metallicities for red giant stars in the globular cluster NGC 6273 based on intermediate resolution GMOS-S spectra of the calcium triplet region. For the 42 radial velocity members with reliable calcium triplet line strength measurements, we obtain metallicities, [Fe/H], using calibrations established from standard globular clusters. We confirm the presence of an intrinsic abundance dispersion identified by Johnson et al. (2015). The total range in [Fe/H] is  $\sim 1.0$  dex and after taking into account the measurement errors, the intrinsic abundance dispersion is  $\sigma_{\text{int}}[\text{Fe}/\text{H}] = 0.17$  dex. Among the Galactic globular clusters, the abundance dispersion in NGC 6273 is only exceeded by  $\omega$  Cen, which is regarded as the remnant of a disrupted dwarf galaxy, and M 54, which is the nuclear star cluster of the Sagittarius dwarf galaxy. If these three globular clusters share the same formation mechanism, then NGC 6273 may also be the remnant nucleus of a disrupted dwarf galaxy.

**Key words:** stars: abundances stars: Population II globular clusters: general globular clusters: individual: NGC 6273.

## 1 INTRODUCTION

The Milky Way Galaxy’s most massive globular cluster,  $\omega$  Centauri, harbours a large star-to-star variation in metallicity, [Fe/H]<sup>1</sup>, spanning at least a factor of 10 (e.g., Freeman & Rodgers 1975; Norris & Da Costa 1995). For the light,  $\alpha$ -, Fe-peak and slow neutron-capture process (*s*-process) elements,  $\omega$  Cen also exhibits a complex distribution in abundance ratios and [X/Fe] (e.g., Smith et al. 2000; Cunha et al. 2002; Stanford et al. 2007; Johnson & Pilachowski 2010; D’Orazi et al. 2011; Marino et al. 2011a; Pancino et al. 2011). That is,  $\omega$  Cen has experienced a complex chemical enrichment history and has

retained ejecta from asymptotic giant branch (AGB) stars as well as from Type Ia and Type II supernovae (Romano et al. 2007; Marcolini et al. 2007). In contrast, the majority of Galactic globular clusters do not exhibit star-to-star variations in metallicity beyond the measurement uncertainties (e.g., Carretta et al. 2009a). At present, arguably the most plausible explanation for  $\omega$  Cen is that it is the surviving nucleus of an accreted dwarf galaxy (Freeman 1993; Lee et al. 1999; Bekki & Freeman 2003).

As recently as 2007,  $\omega$  Centauri was the only globular cluster for which there was undisputed evidence for a metallicity variation. Within the past few years, however, abundance dispersions in Fe-peak and/or *s*-process elements have been reported in a number of globular clusters including NGC 1851 (Yong & Grundahl 2008; Villanova, Geisler & Piotto 2010; Carretta et al. 2011; Gratton et al. 2012; Marino et al. 2014), M 22 (Marino et al. 2009, 2011b; Da Costa et al. 2009; Roederer, Marino & Sneden 2011), Terzan 5 (Ferraro et al. 2009; Origlia et al. 2011, 2013), M 54 (Carretta et al. 2010a,b), M 75 (Kacharov, Koch & McWilliam 2013), NGC 5824 (Da Costa, Held & Saviane 2014), M 2 (Yong et al. 2014) and NGC 5286 (Marino et al. 2015). (Results for

<sup>\*</sup> Based on observations obtained at the Gemini Observatory, which is operated by the Association of Universities for Research in Astronomy, Inc., under a cooperative agreement with the NSF on behalf of the Gemini partnership: the National Science Foundation (United States), the National Research Council (Canada), CONICYT (Chile), the Australian Research Council (Australia), Ministério da Ciência, Tecnologia e Inovação (Brazil) and Ministerio de Ciencia, Tecnología e Innovación Productiva (Argentina).  
<sup>†</sup> E-mail: david.yong@anu.edu.au

<sup>1</sup> We use the standard spectroscopic notation;  $[\text{Fe}/\text{H}] = \log_{10}(N_{\text{Fe}}/N_{\text{H}})_{\star} - \log_{10}(N_{\text{Fe}}/N_{\text{H}})_{\odot}$

some of these clusters have been challenged by, e.g., Mucciarelli et al. 2015 and Roederer et al. 2016.)

It was recognised that these objects (along with  $\omega$  Cen), are preferentially among the most luminous (i.e., massive) of the Galaxy’s globular clusters, and that many have an extended horizontal branch with extremely blue stars (Lee, Gim & Casetti-Dinescu 2007). Some, if not all, of these objects could be the remnants of dwarf galaxies (Bekki & Yong 2012; Da Costa 2015; Marino et al. 2015). In particular, M 54 is currently the nuclear star cluster of the Sagittarius (Sgr) dwarf spheroidal galaxy (dSph). Carretta et al. (2010b) proposed that when the Sgr dSph is tidally disrupted, the compact remnant of the M 54+Sgr system will resemble  $\omega$  Cen. Therefore, the identification of additional globular clusters with intrinsic abundance dispersions in Fe-peak elements may have important consequences for our understanding of Galactic evolution. In order to complete the characterisation of the Galactic globular cluster system and possibly identify new clusters with abundance dispersions in Fe-peak elements, the most promising candidates to investigate are the most luminous globular clusters with extended blue horizontal branches.

NGC 6273 (M 19) has an extended blue horizontal branch and with  $M_V = -9.1$ , it is the 10th most luminous Galactic globular cluster (Harris 1996, updated December 2010) and lies near the Galactic bulge. Proper-motion analysis indicates that it is an inner halo globular cluster (Casetti-Dinescu et al. 2010). Observations by Johnson et al. (2015, hereafter J15) revealed an intrinsic variation in Fe-peak and s-process element abundances. J15 found a “metal-poor” population (9 stars,  $\langle[\text{Fe}/\text{H}]\rangle = -1.75$ ), a “metal-rich” population (8 stars,  $\langle[\text{Fe}/\text{H}]\rangle = -1.51$ ) and one “anomalous” star with  $[\text{Fe}/\text{H}] = -1.30$ . The “metal-rich” population had enhanced ratios of the s-process element La compared to the “metal-poor” population,  $\langle[\text{La}/\text{Fe}]\rangle = +0.16$  and  $\langle[\text{La}/\text{Fe}]\rangle = +0.48$ , respectively. Therefore, NGC 6273 has experienced a complex chemical enrichment history with contributions from Type II supernovae and AGB stars. Narrowband Ca photometry by Han et al. (2015) supports the results from J15. The goal of this work is to study a large sample of red giant branch (RGB) stars in NGC 6273 in order to confirm and quantify the abundance dispersion. In Section 2 we describe the sample selection, observations, data reduction and analysis. The results are presented in Section 3. Sections 4 and 5 include our discussion and conclusions.

## 2 SAMPLE SELECTION, OBSERVATIONS, REDUCTION AND ANALYSIS

Program stars (see Table 1) were selected from  $JK$  colour-magnitude diagrams (CMD) using 2MASS photometry (Skrutskie et al. 2006). All targets occupy plausible locations in the  $J-K$  vs.  $K$  CMD. Specifically, we required  $0.68 \leq J-K \leq 1.2$  and  $8.57^2 \leq K \leq 13.0$  (see Figure 1). Furthermore, all program stars were required to have “AAA” 2MASS photometric quality flags and to lie within 3 arcmin of the cluster centre.

<sup>2</sup> This value corresponds to the tip of the RGB (Valenti, Ferraro & Origlia 2007).

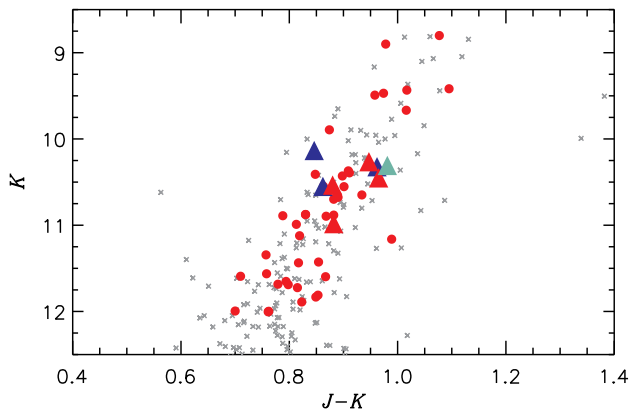


**Figure 1.**  $J-K$  colour-magnitude diagram for NGC 6273 based on 2MASS photometry (Skrutskie et al. 2006). All objects lie within a radius of 3 arcmin and have AAA photometric quality flags. Red circles are likely radial velocity members with reliable Ca II triplet EW measurements. The blue, red and aqua triangles are metal-poor, metal-rich and anomalous stars, respectively, from Johnson et al. (2015).

Observations of the program stars were obtained using the GMOS-S multi-object spectrograph (Hook et al. 2004) at the Gemini-S telescope in queue mode (GS-2012A-Q-58). All observations were taken on 2012 May 05 and the set-up was identical to that of Da Costa, Held & Saviane (2014). We used the R831 grating and the RG610 filter with central wavelengths of 8550 Å and 8600 Å (wavelength coverage was typically from  $\sim 7500$  Å to  $\sim 9000$  Å). Since there are gaps between the three GMOS-S CCDs, observations at two different central wavelengths ensures that the Ca II infrared triplet lines can be measured in at least one of the two settings. Each GMOS mask had slit widths of 1 arcsec and slit lengths of 10 arcsec to facilitate sky and background subtraction. A total of 92 candidate RGB stars were observed across six masks. Two stars (17024132-2613517 and 17024717-2615107) were common to two masks and a total of 21 stars from J15 were included across five masks. Masks 1, 2 and 3 concentrated on brighter targets ( $J \leq 11.7$ ) and the total exposure time per mask was 240 sec (one 120 sec exposure for each of the two central wavelengths). Masks 4, 5 and 6 concentrated on fainter targets ( $J \geq 11.5$ ) and the total exposure time per mask was 960 sec (one 480 sec exposure for each central wavelength). Each observation was preceded, or followed, by a flat-field integration. Arc lamp exposures for each mask were also obtained.

Data reduction was performed using IRAF<sup>3</sup> Gemini package scripts. The final wavelength-calibrated, sky-subtracted spectra have a resolution of  $\sim 3.5$  Å and a (binned) pixel scale of 0.68 Å per pixel (see Figures 2 and 3). The signal-to-noise ratios (S/N), based on the photon counts for a given central wavelength, exceed 100 per pixel for all but three objects with an average value of 170 and a maximum value of 280.

<sup>3</sup> IRAF is distributed by the National Optical Astronomy Observatories, which are operated by the Association of Universities for Research in Astronomy, Inc., under cooperative agreement with the National Science Foundation.

**Table 1.** Program stars.

Name (2MASS)	RA (J2000)	Dec (J2000)	Mask	<i>J</i>	<i>H</i>	<i>K</i>
17022878-2614320	255.61995	-26.24223	1	11.304	10.556	10.393
17023192-2614177	255.63304	-26.23827	1	10.451	9.666	9.434
17023394-2616196	255.64145	-26.27213	1	10.444	9.725	9.470
17023460-2616038	255.64418	-26.26775	1	11.581	10.897	10.699
17023481-2617152	255.64505	-26.28756	1	11.415	10.681	10.535

This table is published in its entirety in the electronic edition of the paper. A portion is shown here for guidance regarding its form and content.

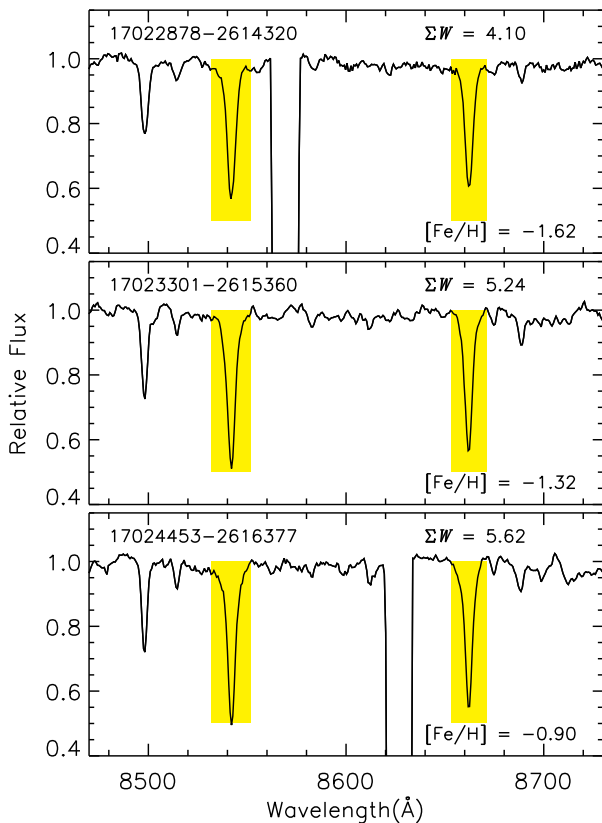


**Figure 2.** A portion of the spectra with central wavelength 8550 Å for three stars with similar *K* magnitudes, all studied by J15, ordered by increasing metallicity. The positions of the 8542 Å and 8662 Å Ca II lines are indicated in yellow. The sum of the equivalent widths,  $\Sigma W$ , is shown in each panel along with the final metallicity. In the upper and lower panels, the regions with zero flux are due to gaps between the CCDs.

As noted by Da Costa, Held & Saviane (2014), the GMOS-S CCDs (at the time of the observations) are affected by strong fringing longward of  $\sim 7000$  Å. The main purpose of these spectra is to measure radial velocities and metallicities based on the strength of the Ca II triplet features. Therefore, even though the spectra have high S/N, the accuracy of the equivalent width measurements is limited by the large amplitude fringing rather than the photon counts (see Figures 2 and 3). Consequently, we treated the spectra taken at the two different central wavelengths independently rather than co-adding them. For spectra of the same star taken with different central wavelengths, the cal-

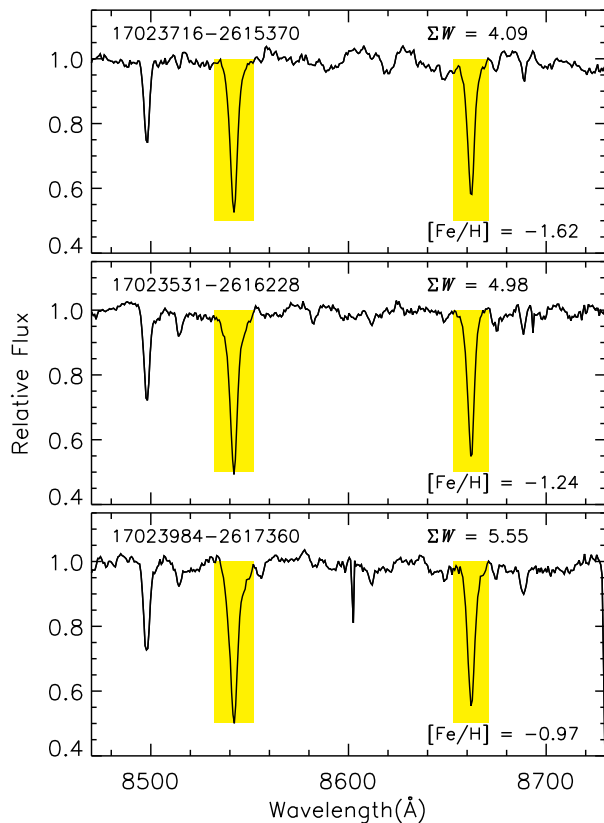


**Figure 3.** Same as Figure 2 but for three different (fainter) stars with central wavelength 8600 Å.

cium triplet lines will fall at different locations on the CCD and be subject to different fringing patterns. As we shall describe later, for each star we will compare the equivalent width measurements from the two spectra and select only those stars for which there is good agreement.

Radial velocities were measured from the wavelengths of the three calcium triplet lines. In a given spectrum, the radial velocity from the three lines were in good agreement and were averaged. For a given star, the radial velocities from the spectra taken with different central wavelengths (8550 Å and 8600 Å) were also in good agreement (maximum absolute difference of  $3.7 \text{ km s}^{-1}$  between the two spectra) and were averaged to produce the final radial velocity.

The zero-points for the radial velocity measurements, however, are not reliable because the arc lamp exposures were taken during the daytime (and for Mask 1, the arc lamp exposures were taken two days after the science observa-

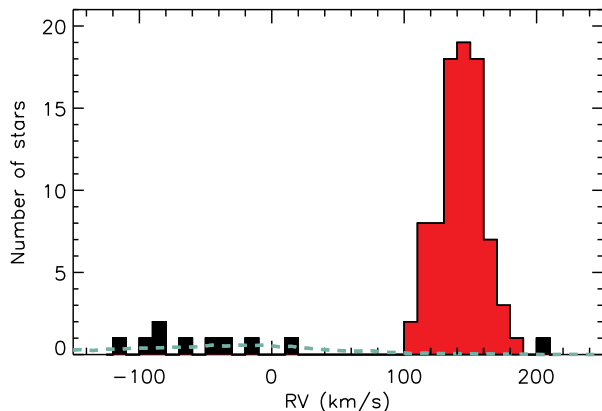


**Figure 4.** Distribution of radial velocities. Stars outside the radial velocity range  $100\text{--}190\text{ km s}^{-1}$  were regarded as non-members. The aqua dashed line is the predicted distribution of field stars from the Besançon model (Robin et al. 2003), normalised to the number of stars with  $RV < 100\text{ km s}^{-1}$ .

tions). Two stars, 17024132-2613517 and 17024717-2615107, were observed in Masks 1 and 4 and the radial velocities differed by  $5.5$  and  $15.3\text{ km s}^{-1}$ , respectively, between the two masks. Fortunately, for Masks 1 through 5, we had six, five, five, four and one star, respectively, in common with J15. By comparing our radial velocities with those of J15, we could place our measurements onto their scale. The minimum and maximum velocity shifts applied to a given mask were  $-7.2$  and  $+5.7\text{ km s}^{-1}$ , respectively. For Mask 6, however, there were no stars in common with J15 and so we shifted the velocities in Mask 6 by  $+16.4\text{ km s}^{-1}$  to match the average value obtained from Masks 1 through 5. Therefore, we regard the uncertainty in any given radial velocity measurement to be  $\sim 15\text{ km s}^{-1}$ .

In Figure 4, we plot the distribution of radial velocities for the program stars. Most of the data lie near  $+145\text{ km s}^{-1}$  and we reject stars with  $RV \leq +100\text{ km s}^{-1}$  and  $RV \geq +190\text{ km s}^{-1}$ . For the stars we regard to be radial velocity members, we find an average radial velocity of  $+144.1\text{ km s}^{-1}$  (the average value in J15 is  $+144.5\text{ km s}^{-1}$ ). While the radial velocity measurements (see Table 2) can help to identify non-members, we cannot obtain a meaningful velocity dispersion from our GMOS-S spectra.

To estimate field contamination, we used the Besançon model (Robin et al. 2003). We considered all stars within one square degree centered on NGC 6273 and only accepted stars with  $0.68 \leq J - K \leq 1.2$  and  $8.57 \leq K \leq 13.0$ . In Figure 4, we overplot the predicted distribution of field stars, normalised to the number of program stars with  $RV < 100\text{ km s}^{-1}$ , i.e., non-members. We therefore expect minor contamination from field stars, only  $\sim 1$  star with  $+100 \leq RV \leq +200\text{ km s}^{-1}$ .

Equivalent widths of the calcium triplet lines were measured by fitting Voigt profiles using routines in IRAF adopting the definitions in Armandroff & Da Costa (1991). For a given star, we could measure the strengths of the  $8542\text{ \AA}$  and  $8662\text{ \AA}$  Ca II lines in the spectra taken with central wavelengths  $8550\text{ \AA}$  and  $8600\text{ \AA}$  (see Table 2). For a given central wavelength, we could then add the equivalent widths for the  $8542\text{ \AA}$  and  $8662\text{ \AA}$  lines to produce  $\Sigma W$ . For each star, we can plot the difference in  $\Sigma W$  between the spectra taken

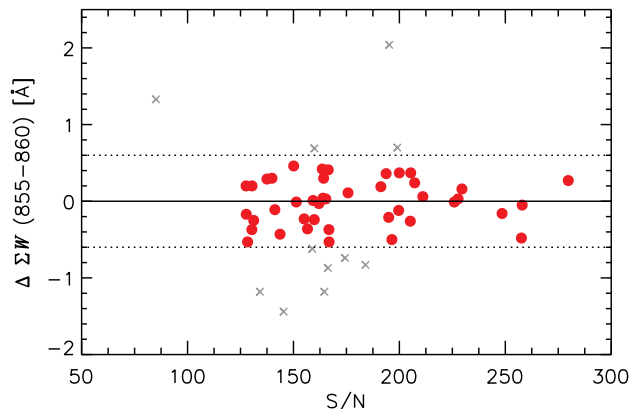


**Figure 5.** Difference in  $\Sigma W$  between the  $8550\text{ \AA}$  and  $8600\text{ \AA}$  spectra versus S/N for each program star for which measurements of  $EW_{8542}$  and  $EW_{8662}$  could be obtained from both sets of spectra. Filled red circles are stars with  $|\Delta\Sigma W| \leq 0.6\text{ \AA}$ .

with central wavelengths  $8550\text{ \AA}$  and  $8600\text{ \AA}$  as a function of S/N (see Figure 5). Only stars for which we were able to measure both lines in both spectra are included in this figure (and we have excluded radial velocity non-members). As in Da Costa, Held & Saviane (2014), while there is reasonable agreement in the two measurements of  $\Sigma W$  for most stars, the difference can be substantial for some stars and persists despite the very high S/N. We attribute these differences to fringing. We arbitrarily adopt a cutoff of  $|\Delta\Sigma W| = 0.6\text{ \AA}$  and  $S/N \geq 100$  in order to select only the best spectra. For these 42 stars, the average difference in  $\Sigma W$  between the  $8550\text{ \AA}$  and  $8600\text{ \AA}$  spectra is  $-0.01 \pm 0.05\text{ \AA}$  ( $\sigma = 0.29$ ). For these stars, we average the measurements from the  $8550\text{ \AA}$  and  $8600\text{ \AA}$  spectra to obtain the final  $\Sigma W$  (see Table 2).

### 3 RESULTS

In Figure 6, we plot the sum of the  $8542\text{ \AA}$  and  $8662\text{ \AA}$  equivalent widths ( $\Sigma W$ ) as a function of the magnitude difference from the horizontal branch for 42 stars as filled red circles. We applied a line-strength correction factor of 1.046 following Da Costa, Held & Saviane (2014) and adopted  $K(\text{HB}) = 12.85$  from Valenti, Ferraro & Origlia (2007). We also include comparison globular clusters from Mauro et al. (2014). Of the 21 stars in common with J15, eight have metallicities from J15 and we overplot those objects as large filled triangles. Of those eight objects, three are from the “metal-poor” population (blue), four are from the “metal-rich” population (red) and the sole “anomalous” star is included (aqua). We caution that for five of these eight stars in common with J15, we were unable to measure equivalent widths for the  $8542\text{ \AA}$  and  $8662\text{ \AA}$  lines in both spectra ( $8550\text{ \AA}$  and  $8600\text{ \AA}$ ). Therefore we were unable to compare  $\Sigma W$  between the  $8550\text{ \AA}$  and  $8600\text{ \AA}$  spectra and so the  $\Sigma W$  measurements for those five stars may have larger errors than for the 42 program stars. We will comment on these stars later in this section.

Following Mauro et al. (2014), we use the  $K$  magnitude rather than the  $V$  magnitude in Figure 6. The advantages to this approach are that extinction and differential reddening in the  $K$  band are much lower when compared to the  $V$  band. Additionally, the relatively flat slope of the

**Table 2.** Radial velocities, equivalent widths and metallicities.

Name (2MASS)	Mask	RV km s <sup>-1</sup>	EW <sub>8542</sub> (8550 Å) Å	EW <sub>8542</sub> (8600 Å) Å	EW <sub>8662</sub> (8550 Å) Å	EW <sub>8662</sub> (8600 Å) Å	ΣW Å	σΣW Å	W' Å	[Fe/H] dex	σ[Fe/H] dex
17022878-2614320	1	144	2.24	2.65	1.86	1.88	4.32	0.21	3.57	-1.62	0.09
17023192-2614177	1	129	2.83	3.16	2.24	1.85	5.05	0.26	3.97	-1.45	0.13
17023394-2616196	1	155	2.70	2.50	1.75	1.92	4.44	0.13	3.34	-1.71	0.06
17023460-2616038	1	164	2.54	2.47	1.64	2.08	4.37	0.22	3.74	-1.55	0.10
17023481-2617152	1	155	3.26	2.72	2.03	1.79	4.90	0.30	...	...	...

This table is published in its entirety in the electronic edition of the paper. A portion is shown here for guidance regarding its form and content.

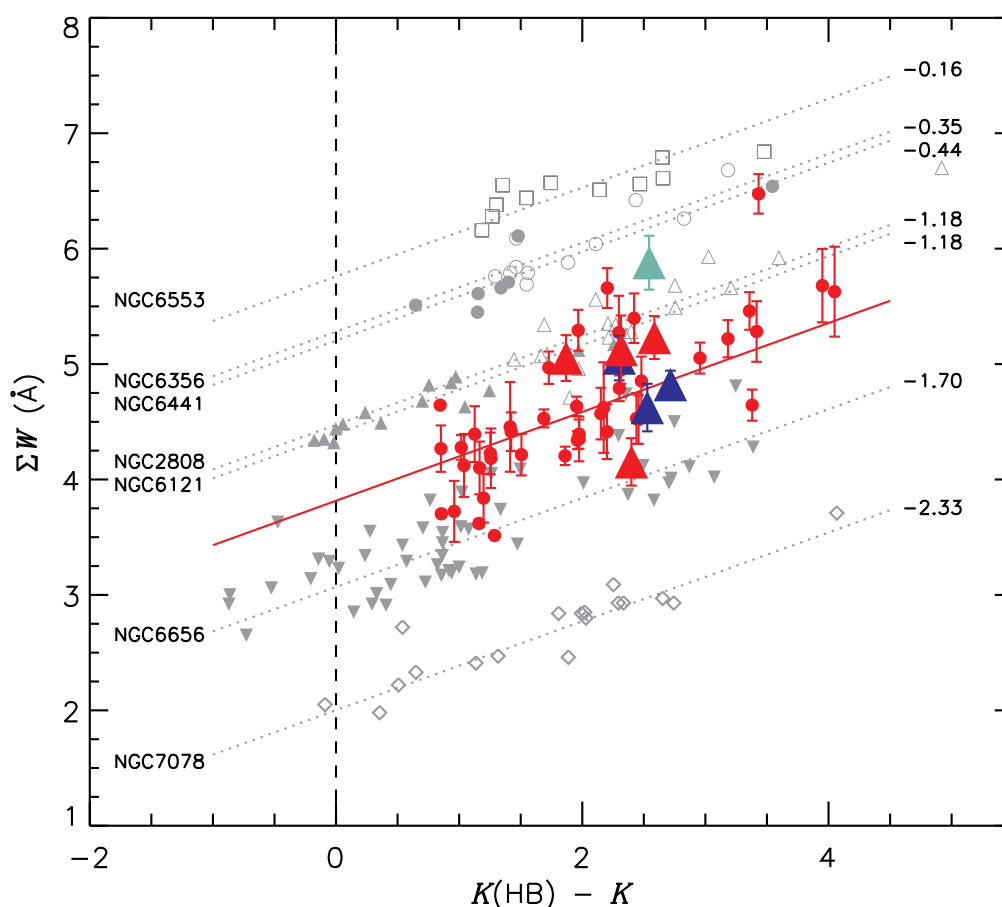


**Figure 6.** Sum of the 8542 Å and 8662 Å equivalent widths ( $\Sigma W$ ) as a function of the magnitude difference from the horizontal branch for 42 program stars (red filled circles). The red solid line is the average value when imposing a gradient of  $-0.385$  Å/mag. The large triangles are eight stars with metallicity measurements from J15. Comparison globular clusters (individual stars and the best fitting line) from Mauro et al. (2014) are overplotted.

$\Sigma W$  vs.  $K(\text{HB}) - K$  relation ( $-0.385$  Å/mag compared to  $-0.63$  Å/mag for the optical relation) means that errors arising from photometry, distance and/or reddening will have a smaller impact upon the derived metallicities.

To obtain metallicities, we adopted the approach of Mauro et al. (2014) and assumed the relation  $\Sigma W = 0.385[K(\text{HB}) - K] + W'$ . For each star, we can then obtain the reduced equivalent width,  $W'$ . For the 42 stars shown in Figure 6, we find an average reduced equivalent width of  $\langle W' \rangle = 3.86 \pm 0.07$  Å ( $\sigma = 0.42$  Å). Note that the stan-

dard deviation of  $0.42$  Å cannot be attributed entirely to the difference in  $\Sigma W$  measured from the two different settings, 8550 Å and 8600 Å, nor to the uncertainties in  $\Sigma W$  (the average uncertainty is  $0.19 \pm 0.01$  Å). Therefore, there is an intrinsic spread in  $\Sigma W$ , i.e., Ca II line strengths, in NGC 6273.

To convert the reduced equivalent widths into metallicities, we use the following relation from Mauro et al. (2014) which is calibrated by the observed line strengths in standard globular clusters with metallicities on the

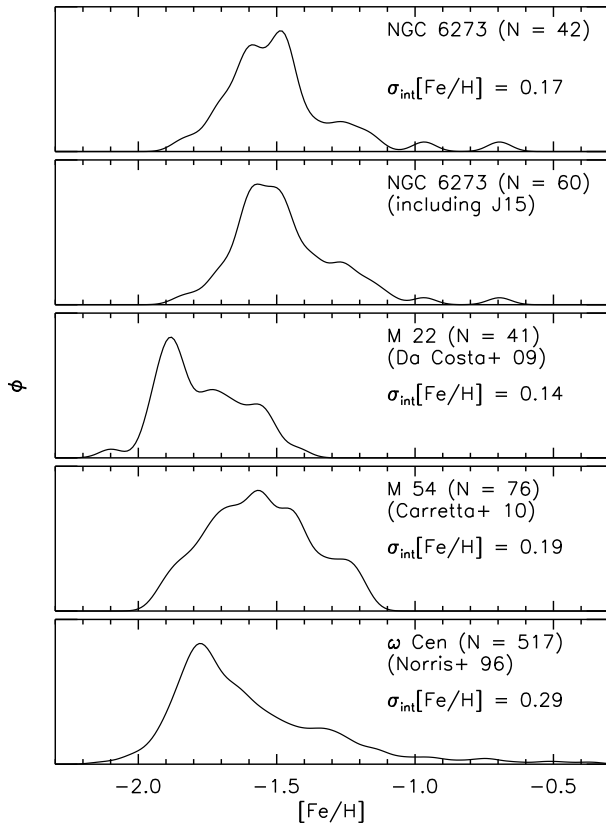


**Figure 7.** Abundance distributions (in generalised histogram form) for NGC 6273 (upper two panels), M 22 (third panel, data from Da Costa et al. 2009), M 54 (fourth panel, data from Carretta et al. 2010a) and  $\omega$  Cen (lower panel, data from Norris, Freeman & Mighell 1996, see text for details). The second panel includes all stars from J15 but with metallicities shifted by +0.20 dex (see text for details). The intrinsic dispersion is written in each panel (see text for details) as well as the number of stars.

Carretta et al. (2009b) abundance scale:  $[\text{Fe}/\text{H}] = -4.61 + 1.842\langle W' \rangle - 0.4428\langle W' \rangle^2 + 0.04517\langle W' \rangle^3$ . Using this calibration, we obtain an average metallicity of  $[\text{Fe}/\text{H}] = -1.48 \pm 0.03$  ( $\sigma = 0.21$ ). We plot the metallicity distribution in Figure 7, upper panel, as a generalised histogram in which each data point is represented by a unit Gaussian of width 0.10 dex. (The average error in  $[\text{Fe}/\text{H}]$  is close to 0.10 dex).

We now seek to quantify the abundance dispersion. For the 42 program stars, the standard deviation for  $W'$  is 0.42 Å and the average error is 0.19 Å. When taking into account the error, the intrinsic spread in  $W'$  is therefore  $\sim 0.38$  Å. At the metallicity of NGC 6273, that intrinsic spread in reduced equivalent width translates into an intrinsic abundance spread of  $\sigma_{\text{int}}[\text{Fe}/\text{H}] = 0.17$  dex. We therefore confirm the results of J15 who reported a very similar value of  $\sigma[\text{Fe}/\text{H}] = 0.16$  dex and an average metallicity of  $[\text{Fe}/\text{H}] = -1.62$ .

In order to select stars with reliable calcium triplet line strength measurements, we required  $\Sigma W$  to be in good agreement between the 8550 Å and 8600 Å observations;  $|\Delta \Sigma W| \leq 0.6$  Å as seen in Figure 5. Had we adopted a more stringent cutoff of  $|\Delta \Sigma W| \leq 0.4$  Å, our results and conclusions would be essentially unchanged: for the 34 stars that

**Table 3.** Equivalent widths and metallicities for eight stars from J15.

Name (2MASS)	$W'$	$\sigma W'$	$[\text{Fe}/\text{H}]$	$\sigma[\text{Fe}/\text{H}]$	$[\text{Fe}/\text{H}]$
	Å	Å	dex	dex	(J15) dex
Metal-poor population					
17024618-2615261	3.65	0.21	-1.59	0.09	-1.76
17023856-2617209	3.78	0.12	-1.54	0.05	-1.80
17023158-2617259	4.17	0.19	-1.35	0.10	-1.80
Metal-rich population					
17023481-2617152	4.23	0.30	-1.32	0.16	-1.44
17023301-2615360	4.23	0.19	-1.32	0.11	-1.37
17024016-2616096	3.23	0.21	-1.76	0.08	-1.60
17024326-2617504	4.33	0.20	-1.27	0.12	-1.55
Anomalous population					
17024453-2616377	4.90	0.23	-0.90	0.19	-1.30

meet that criterion, the standard deviation in  $W'$  is 0.46 Å and the average error in  $\Sigma W$  is 0.17 Å, i.e., the dispersion in  $W'$  cannot be explained by errors in  $\Sigma W$  alone. Instead, the intrinsic spread in  $W'$  is 0.42 Å and this translates into an intrinsic abundance spread of  $\sigma_{\text{int}}[\text{Fe}/\text{H}] = 0.19$  dex.

NGC 6273 suffers from large and variable reddening,  $E(B-V) = 0.32$  and  $\Delta E(B-V) \sim 0.3$  (Alonso-García et al. 2012). One possibility is that differential reddening is responsible (in part or in whole) for the dispersion in  $W'$  and metallicity dispersion. To check this possibility, we used the differential reddening map for NGC 6273 from Alonso-García et al. (2012). For each program star, we averaged the differential reddening values within 5 arcsec. The average value was  $\Delta E(B-V) = 0.015 \pm 0.006$  ( $\sigma = 0.068$ ) with minimum and maximum values of -0.100 and 0.174. Assuming  $A_K = 0.34E(B-V)$ , the standard deviation in  $W'$  is unchanged and therefore, differential reddening as high as  $\Delta E(B-V) = \sim 0.27$  does not affect the derived metallicities. As noted, using the  $K$  magnitude rather than the  $V$  magnitude greatly reduces the effect of differential reddening and the slope of the  $\Sigma W$  vs.  $K(\text{HB})-K$  relation is flatter than the corresponding optical trend.

Recall that we also observed eight stars with metallicities from J15. For five of these objects, however, we could not measure the equivalent widths for 8542 Å and 8662 Å in both spectra. While their  $\Sigma W$  measurements may have larger uncertainties, we can obtain metallicities and compare our values with J15 (see Table 3). The average difference is  $\Delta[\text{Fe}/\text{H}] = 0.20 \pm 0.07$  ( $\sigma = 0.20$  dex), with our values being higher than those of J15. On our abundance scale, the three “metal-poor” stars and four “metal-rich” stars from J15 have average metallicities of  $[\text{Fe}/\text{H}] = -1.49$  and  $[\text{Fe}/\text{H}] = -1.42$ , respectively. The “anomalous” star has  $[\text{Fe}/\text{H}] = -0.90$ . In the second panel of Figure 7, we combine our program stars with all stars from J15 but we shift their metallicities by +0.20 dex to match our scale. The upper two panels exhibit very similar abundance distributions. That is, including or excluding the J15 stars does not affect our results, namely, that there is an intrinsic abundance dispersion in NGC 6273.

Of particular interest is the possibility that NGC 6273 hosts a third, “anomalous”, population. J15 identified one “anomalous” star, 17024453-2616377, with  $[\text{Fe}/\text{H}]$

=  $-1.30$  on their abundance scale. That star has  $[\text{Fe}/\text{H}] = -0.90$  on our abundance scale. We identify four additional stars with  $[\text{Fe}/\text{H}] > -1.2$ : 17023649-2615229 ( $[\text{Fe}/\text{H}] = -1.19$ ), 17023685-2616217 ( $[\text{Fe}/\text{H}] = -1.15$ ), 17023984-2617360 ( $[\text{Fe}/\text{H}] = -0.97$ ) and 17023595-2615342 ( $[\text{Fe}/\text{H}] = -0.70$ ). Assuming that at least one of those stars is a genuine cluster member (recall that the Besançon model predicted only  $\sim 1$  field star contaminant), then our spectra confirm that NGC 6273 hosts an “anomalous” population, i.e., a high metallicity tail.

In Figure 8, we separate the program stars based on their metallicity into two groups to investigate whether there are any systematic differences in their spatial distributions, location in the CMD or radial velocity distributions. We arbitrarily choose  $[\text{Fe}/\text{H}] = -1.50$  as the boundary between the two groups. From this figure, the spatial and radial velocity distributions for the two populations overlap. Regarding the CMD, while we would expect the more metal-rich stars to be redder at a given  $K$  magnitude when compared to the more metal-poor stars, we find no significant differences in colour between the two populations.

#### 4 DISCUSSION

We confirm the results from J15 that NGC 6273 harbours an internal abundance dispersion. In the lower three panels of Figure 7, we also plot the metallicity distributions for well-studied globular clusters that also exhibit abundance dispersions, M 22 (Da Costa et al. 2009), M 54 (Carretta et al. 2010a) and  $\omega$  Cen (Norris, Freeman & Mighell 1996)<sup>4</sup>. The same smoothing, FWHM = 0.10 dex, has been applied to all panels in this figure. For M 22 and  $\omega$  Cen, the metallicity measurements were made using intermediate resolution spectra of the Ca II triplet lines, i.e., a similar approach as in this study. For M 54, however, the metallicities are obtained from analysis of individual Fe lines based on high-resolution spectra.

In the upper panel of Figure 7, we write the intrinsic abundance dispersion for NGC 6273 which was computed and described in the previous Section. For M 22 (Da Costa et al. 2009), M 54 (Carretta et al. 2010a) and  $\omega$  Cen (Norris, Freeman & Mighell 1996), the measurement errors are 0.06, 0.02, and 0.05 dex, respectively. To obtain the intrinsic abundance dispersion,  $\sigma_{\text{int}}[\text{Fe}/\text{H}]$ , we assume that the observed standard deviation is the quadratic sum of the measurement error and the intrinsic abundance dispersion, and we write the latter quantity in the bottom three panels. NGC 6273 has  $\sigma_{\text{int}}[\text{Fe}/\text{H}] = 0.17$  dex which is marginally smaller than that of M 54,  $\sigma_{\text{int}}[\text{Fe}/\text{H}] = 0.19$  dex. M 22 has a slightly smaller value,  $\sigma_{\text{int}}[\text{Fe}/\text{H}] = 0.14$ , while  $\omega$  Cen has the highest value,  $\sigma_{\text{int}}[\text{Fe}/\text{H}] = 0.29$  dex.

At low metallicity, the abundance distribution of NGC 6273 rises rapidly in a similar manner as  $\omega$  Cen, but perhaps not as steeply as M 22. For M 54, the abundance distribution appears to rise more slowly compared to the other globular

<sup>4</sup> For the  $\omega$  Cen data, Norris, Freeman & Mighell (1996) calibrate the Ca II line strengths to  $[\text{Ca}/\text{H}]$ , rather than  $[\text{Fe}/\text{H}]$ . Norris & Da Costa (1995) find a mean  $[\text{Ca}/\text{Fe}]$  of +0.39, and we have shifted the Norris, Freeman & Mighell (1996) values by  $-0.39$  dex to obtain  $[\text{Fe}/\text{H}]$ .

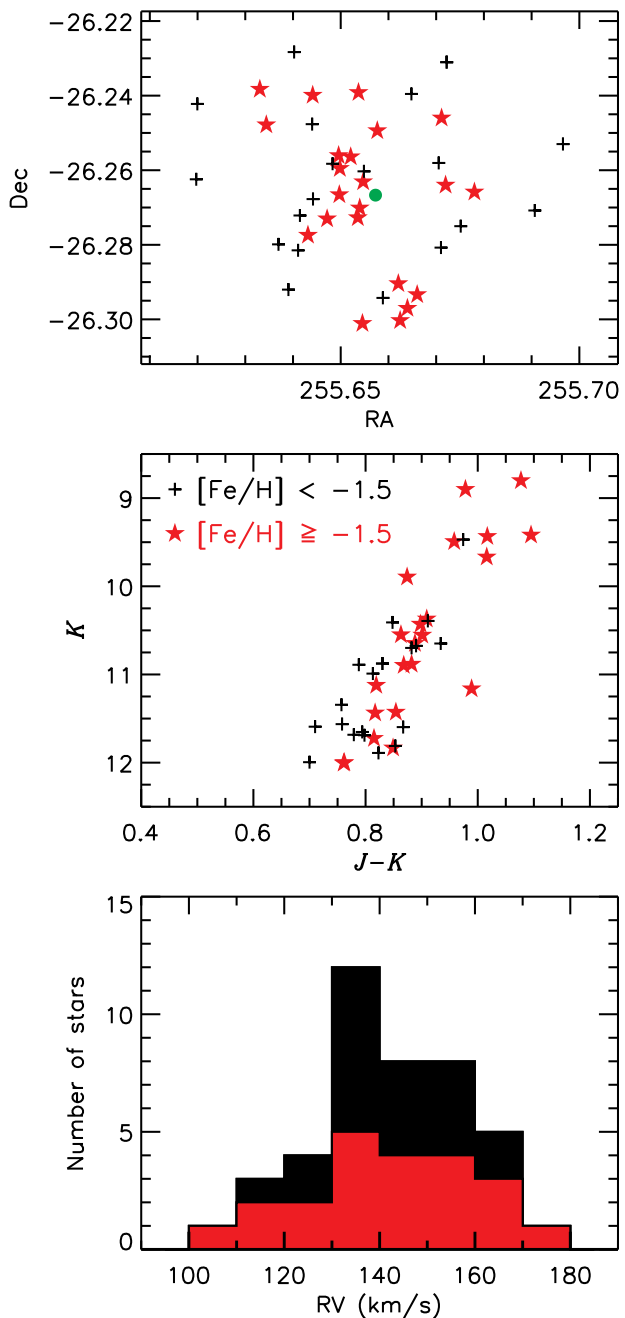


**Figure 8.** Spatial distribution (upper), CMD (middle) and radial velocity distribution (lower). Black crosses and red stars represent objects with  $[\text{Fe}/\text{H}] < -1.5$  and  $[\text{Fe}/\text{H}] \geq -1.5$ , respectively.

clusters. At high metallicity, NGC 6273 has a tail that extends to at least  $[\text{Fe}/\text{H}] = -1.0$ , and perhaps as high as  $[\text{Fe}/\text{H}] = -0.70$ . Overall, the shape of the abundance distribution of NGC 6273 most closely resembles that of  $\omega$  Cen.

We note that Mucciarelli et al. (2015) have challenged the existence of an iron abundance dispersion in M 22 reported by Marino et al. (2009, 2011b) based on high-resolution spectroscopy. Mucciarelli et al. (2015) found that when using surface gravities based on photometry, the  $[\text{Fe}/\text{H}]$  distribution exhibits no spread. They suggested that neglect of non-local thermodynamic equilibrium

(NLTE) effects can produce spurious abundance spreads. For M 22, however, there is also a real spread in Ca II line strengths (Da Costa et al. 2009) which, if not due to metallicity variations, requires an unknown explanation. Recent NLTE calculations for Fe (Bergemann et al. 2012; Lind, Bergemann & Asplund 2012) indicate that for stars with similar stellar parameters, the NLTE corrections are very similar (i.e., the differential NLTE effects are very small). We consider the abundance spreads in M 22 as real given the concordance between the high dispersion results and the Ca II results for this cluster and that the differential NLTE corrections are expected to be negligible.

The increase in *s*-process element abundances with increasing metallicity is a characteristic shared by  $\omega$  Cen, M 22, M 2, NGC 5286 and NGC 6273 and requires contributions from Type II supernovae and AGB stars. The presence of a third, “anomalous”, population at higher metallicity but without *s*-process element enhancements or light element abundance anomalies has only been identified in M 2 (four stars) and NGC 6273 (one star). Clearly, it would be of great interest to examine chemical abundances for a larger suite of elements in the most metal-rich stars of NGC 6273 to establish whether the anomalous populations in these two globular clusters share common characteristics.

It is worth noting that initial observations of the Ca II triplet in the outer halo globular cluster NGC 2419 showed line strength variations (Cohen et al. 2010). Subsequent analyses, however, revealed that this cluster has a single metallicity,  $[\text{Fe}/\text{H}] = \sim -2.1$ , but is highly unusual in that it exhibits very large star-to-star variations for Mg and K (factors of  $\sim 100$ ) (Cohen, Huang & Kirby 2011; Cohen & Kirby 2012; Mucciarelli et al. 2012). Mg is an important electron donor in low mass stars (and thus contributes to the  $\text{H}^-$  continuous opacity), and the large Mg depletion combined with a small star-to-star Ca variation could explain the behaviour of the Ca II triplet lines in NGC 2419 (Cohen & Kirby 2012; Mucciarelli et al. 2012). A similar explanation could possibly also apply to NGC 5824 (Da Costa, Held & Saviane 2014; Roederer et al. 2016). For NGC 6273, however, the calcium line strength variation is larger than in NGC 2419 and NGC 5824, the Mg variation is relatively modest ( $\Delta[\text{Mg}/\text{Fe}] \simeq 0.5$ ; J15) and the overall metallicity is higher. So it seems unlikely that star-to-star Mg variations are driving the calcium line strength variations in NGC 6273.

We reiterate that the most plausible explanation for the origin of  $\omega$  Cen is that it is the surviving nucleus of an accreted dwarf galaxy (Freeman 1993; Lee et al. 1999; Bekki & Freeman 2003). It has been argued that when the Sgr dSph is tidally disrupted by the Milky Way, the remnant of the M 54+Sgr system may closely resemble  $\omega$  Cen (Carretta et al. 2010b). Since  $\omega$  Cen, M 54 and NGC 6273 all exhibit an intrinsic abundance dispersion, it is tempting to suggest that they may all share a similar formation mechanism as the remnant nuclei of disrupted dwarf galaxies. If this is the case, then one might expect to find a diffuse stellar envelope (and/or extratidal stars) surrounding NGC 6273 as is the case for other globular clusters that exhibit abundance dispersions in Fe-peak and/or *s*-process elements including NGC 1851 (Olszewski et al. 2009; Marino et al. 2014; Navin, Martell & Zucker 2015), NGC 5824 (Grillmair et al. 1995), M 2 (Grillmair et al. 1995, Kuzma et al. in prep) and M 22 (Kunder et al. 2014). Identifying such a stellar halo

will be challenging given that NGC 6273 lies near the Galactic bulge and has large and variable reddening,  $E(B - V) = 0.32$  and  $\Delta E(B - V) \sim 0.3$  (Alonso-García et al. 2012).

Finally, two ( $\omega$  Cen and M 22) of the clusters previously known to exhibit variations of the heavy elements Ca and/or Fe are also known to exhibit very large variations in cyanogen and to exhibit large ellipticities (see Norris 1987)<sup>5</sup>. We note then that NGC 6273 exhibits the largest ellipticity of the Galactic globular cluster population ( $\epsilon \sim 0.28$ , White & Shawl 1987). From narrowband Ca photometry, Han et al. (2015) identified a Ca-rich and Ca-poor population in NGC 6273 and measured the CN and CH line strength indices in each population. They found that the Ca-rich population was also enhanced in CN, which is similar to  $\omega$  Cen and M 22 (Norris & Freeman 1983).

## 5 CONCLUSIONS

We confirm that the globular cluster NGC 6273 harbours an intrinsic abundance spread based on intermediate resolution GMOS-S spectra of the line strengths of the Ca II triplet features. The intrinsic abundance dispersion,  $\sigma_{\text{int}}[\text{Fe}/\text{H}] = 0.17$  agrees with the results from J15,  $\sigma[\text{Fe}/\text{H}] = 0.16$ . NGC 6273 therefore has the third largest abundance dispersion after  $\omega$  Cen and M 54 among the Galactic globular clusters. The total range in metallicity is  $\sim 1.0$  dex. We confirm the presence of a high metallicity tail with values reaching above  $[\text{Fe}/\text{H}] = -1.0$  and perhaps up to  $[\text{Fe}/\text{H}] = -0.70$ . Given the similarities in the abundance distribution, we argue that NGC 6273 and  $\omega$  Cen may share the same origin as the nuclei of disrupted dwarf galaxies.

## ACKNOWLEDGMENTS

We thank the anonymous referee for a careful reading of the paper and helpful comments. We gratefully acknowledge support from the Australian Research Council (grants DP0984924, DP120101237, DP120100475, FT140100554 and DP150103294).

## REFERENCES

- Alonso-García J., Mateo M., Sen B., Banerjee M., Catelan M., Minniti D., von Braun K., 2012, *AJ*, 143, 70
- Armandroff T. E., Da Costa G. S., 1991, *AJ*, 101, 1329
- Bekki K., Freeman K. C., 2003, *MNRAS*, 346, L11
- Bekki K., Yong D., 2012, *MNRAS*, 419, 2063
- Bergemann M., Lind K., Collet R., Magic Z., Asplund M., 2012, *MNRAS*, 427, 27
- Carretta E., Bragaglia A., Gratton R., D’Orazi V., Lucatello S., 2009a, *A&A*, 508, 695
- Carretta E. et al., 2010a, *A&A*, 520, A95
- Carretta E. et al., 2010b, *ApJ*, 714, L7
- Carretta E. et al., 2009b, *A&A*, 505, 117

<sup>5</sup> The fact that the third cluster, M 54, has only a small measured ellipticity ( $\epsilon \sim 0.06$ , White & Shawl 1987) may result from projection effects.

- Carretta E., Lucatello S., Gratton R. G., Bragaglia A., D’Orazi V., 2011, *A&A*, 533, A69
- Casetti-Dinescu D. I., Girard T. M., Korchagin V. I., van Altena W. F., López C. E., 2010, *AJ*, 140, 1282
- Cohen J. G., Huang W., Kirby E. N., 2011, *ApJ*, 740, 60
- Cohen J. G., Kirby E. N., 2012, *ApJ*, 760, 86
- Cohen J. G., Kirby E. N., Simon J. D., Geha M., 2010, *ApJ*, 725, 288
- Cunha K., Smith V. V., Suntzeff N. B., Norris J. E., Da Costa G. S., Plez B., 2002, *AJ*, 124, 379
- Da Costa G. S., 2015, "The General Assembly of Galaxy Halos: Structure, Origin and Evolution", *Proceedings of IAU Symposium 317*, eds A. Bragaglia, M. Arnaboldi, M. Rejkuba and D. Romano, (Cambridge: CUP), in press (arXiv:1510.00873)
- Da Costa G. S., Held E. V., Saviane I., 2014, *MNRAS*, 438, 3507
- Da Costa G. S., Held E. V., Saviane I., Gullieuszik M., 2009, *ApJ*, 705, 1481
- D’Orazi V., Gratton R. G., Pancino E., Bragaglia A., Carretta E., Lucatello S., Sneden C., 2011, *A&A*, 534, A29
- Ferraro F. R. et al., 2009, *Nature*, 462, 483
- Freeman K. C., 1993, in *Astronomical Society of the Pacific Conference Series*, Vol. 48, *The Globular Cluster-Galaxy Connection*, Smith G. H., Brodie J. P., eds., p. 608
- Freeman K. C., Rodgers A. W., 1975, *ApJ*, 201, L71
- Gratton R. G., Villanova S., Lucatello S., Sollima A., Geisler D., Carretta E., Cassisi S., Bragaglia A., 2012, *A&A*, 544, A12
- Grillmair C. J., Freeman K. C., Irwin M., Quinn P. J., 1995, *AJ*, 109, 2553
- Han S.-I., Lim D., Seo H., Lee Y.-W., 2015, *ApJ*, 813, L43
- Harris W. E., 1996, *AJ*, 112, 1487
- Hook I. M., Jørgensen I., Allington-Smith J. R., Davies R. L., Metcalfe N., Murowinski R. G., Crampton D., 2004, *PASP*, 116, 425
- Johnson C. I., Pilachowski C. A., 2010, *ApJ*, 722, 1373
- Johnson C. I., Rich R. M., Pilachowski C. A., Caldwell N., Mateo M., Bailey, III J. I., Crane J. D., 2015, *AJ*, 150, 63
- Kacharov N., Koch A., McWilliam A., 2013, *A&A*, 554, A81
- Kunder A. et al., 2014, *A&A*, 572, A30
- Lee Y.-W., Gim H. B., Casetti-Dinescu D. I., 2007, *ApJ*, 661, L49
- Lee Y.-W., Joo J.-M., Sohn Y.-J., Rey S.-C., Lee H.-C., Walker A. R., 1999, *Nature*, 402, 55
- Lind K., Bergemann M., Asplund M., 2012, *MNRAS*, 427, 50
- Marcolini A., Sollima A., D’Ercole A., Gibson B. K., Ferraro F. R., 2007, *MNRAS*, 382, 443
- Marino A. F. et al., 2015, *MNRAS*, 450, 815
- Marino A. F., Milone A. P., Piotto G., Villanova S., Bedin L. R., Bellini A., Renzini A., 2009, *A&A*, 505, 1099
- Marino A. F. et al., 2011a, *ApJ*, 731, 64
- Marino A. F. et al., 2014, *MNRAS*, 442, 3044
- Marino A. F. et al., 2011b, *A&A*, 532, A8
- Mauro F. et al., 2014, *A&A*, 563, A76
- Mucciarelli A., Bellazzini M., Ibata R., Merle T., Chapman S. C., Dalessandro E., Sollima A., 2012, *MNRAS*, 426, 2889
- Mucciarelli A., Lapenna E., Massari D., Pancino E., Stetson P. B., Ferraro F. R., Lanzoni B., Lardo C., 2015, *ApJ*, 809, 128
- Navin C. A., Martell S. L., Zucker D. B., 2015, *MNRAS*, 453, 531
- Norris J., 1987, *ApJ*, 313, L65
- Norris J., Freeman K. C., 1983, *ApJ*, 266, 130
- Norris J. E., Da Costa G. S., 1995, *ApJ*, 447, 680
- Norris J. E., Freeman K. C., Mighell K. J., 1996, *ApJ*, 462, 241
- Olszewski E. W., Saha A., Knezek P., Subramaniam A., de Boer T., Seitzer P., 2009, *AJ*, 138, 1570
- Origlia L., Massari D., Rich R. M., Mucciarelli A., Ferraro F. R., Dalessandro E., Lanzoni B., 2013, *ApJ*, 779, L5
- Origlia L. et al., 2011, *ApJ*, 726, L20
- Pancino E., Mucciarelli A., Sbordone L., Bellazzini M., Pasquini L., Monaco L., Ferraro F. R., 2011, *A&A*, 527, A18
- Robin A. C., Reylé C., Derrière S., Picaud S., 2003, *A&A*, 409, 523
- Roederer I. U., Marino A. F., Sneden C., 2011, *ApJ*, 742, 37
- Roederer I. U., Mateo M., Bailey J. I., Spencer M., Crane J. D., Shtetman S. A., 2016, *MNRAS*, 455, 2417
- Romano D., Matteucci F., Tosi M., Pancino E., Bellazzini M., Ferraro F. R., Limongi M., Sollima A., 2007, *MNRAS*, 376, 405
- Skrutskie M. F. et al., 2006, *AJ*, 131, 1163
- Smith V. V., Suntzeff N. B., Cunha K., Gallino R., Busso M., Lambert D. L., Straniero O., 2000, *AJ*, 119, 1239
- Stanford L. M., Da Costa G. S., Norris J. E., Cannon R. D., 2007, *ApJ*, 667, 911
- Valenti E., Ferraro F. R., Origlia L., 2007, *AJ*, 133, 1287
- Villanova S., Geisler D., Piotto G., 2010, *ApJ*, 722, L18
- White R. E., Shawl S. J., 1987, *ApJ*, 317, 246
- Yong D., Grundahl F., 2008, *ApJ*, 672, L29
- Yong D. et al., 2014, *MNRAS*, 441, 3396